Chapter 5
Development of a GIS-Based 3D Slope Stability Analysis System for Rainfall-Induced Landslide Hazard Assessment

Cheng Qiu and Yasuhiro Mitani

Abstract The assessment of landslide hazard should give answers to three key questions: the location, the magnitude, and the occurrence time of potential failures. This paper proposes a GIS-aided 3D methodology for quantitative assessment of regional landslide hazard and prediction of the three key questions. A revised 3D slope stability model is developed by coupling a dynamic rainfall infiltration model with a 3D limit equilibrium approach. To define the study object of the 3D model in regional assessment, an automatic methodology of slope-unit division is developed by using GIS hydraulic analysis functions. The location and shape of unknown slip surface(s) are identified by means of minimizing the 3D safety factor through an iterative procedure, based on a Monte Carlo simulation for the 3D shape of ellipsoid. Executing the searching calculation for each slope unit during rainfall can result in changing distribution of the critical slip surface(s) as well as their occurrence time related with rainfall. Incorporating all proposed methods, a standalone GIS system, called 3D slope stability analysis GIS system (3DSSAGS), is developed based on the Component Object Model technology. In this system, all the professional analyses are embedded within GIS for efficient use of GIS functions.

Keywords Landslide hazard · 3D slope stability model · Rainfall infiltration · GIS

C. Qiu (✉)
Hydro-soft Technology Institute Co., Ltd., Shiroyama Trust Tower 31F,
Toranomon 4-3-1, Minato-ku, Tokyo, Japan
e-mail: qiucheng321@gmail.com

Y. Mitani
Kyushu University, Motooka 744, Nishi-ku, Fukuoka, Japan
e-mail: mitani@doc.kyushu-u.ac.jp

5.1 Introduction

The assessment of landslide hazard has become a topic of major interests for both geoscientists and engineering professionals as well as for local communities and administrations in many parts of the world. Governments and research institutions worldwide have long attempted to assess landslide hazard and risks and to portray its spatial distribution in maps. Within this framework, earth sciences, and geomorphology in particular, may play a relevant role in assessing areas at high landslide hazard and in helping to mitigate the associated risk, providing a valuable aid to a sustainable progress.

Landslide hazard is defined as the probability of occurrence of a potentially damaging phenomenon within a given area and in a given period of time by Varnes (1984). The definition incorporates the concepts of magnitude, geographical location, and occurrence time. The first refers to the "dimension" or "intensity" of the natural phenomenon which conditions its behavior and destructive power; the second implies the ability to identify the place where the phenomenon may occur; the third refers to the temporal prediction of the event. Therefore, landslide hazard assessment study, which is commonly used for hazard mitigation, should give answers to three key questions: the magnitude, the location, and the occurrence time of a dangerous process.

However, so far, there are few reliable methodologies available for giving the answers. Historical information about landslides, with a more or less precise indication of slopes affected by instability and the dates of the active stages of the landslides, is important for an accurate temporal assessment relating data on triggering rainfall or on earthquakes to the resulting landslides. Although it is possible to observe relationships between current landslides and rainfall or earthquakes, the number of landslides for which temporal information is available may be so few that it is impossible to undertake a quantitative landslide hazard assessment.

On the other hand, once the slope geometry and subsoil conditions have been determined, the stability of a slope may be assessed using the deterministic methodologies. Most of the deterministic models are based on the limiting equilibrium approach for a two-dimensional (2D) model. The results of the 2D analysis are usually conservative, and although more expensive, three-dimensional (3D) analysis tends to increase the accuracy of result. It is well known that a 3D situation may become important in cases that the geometry of a slope varies significantly in the lateral direction, the material properties are highly anisotropic, or the slope is locally loaded (Chang 2002). Since the mid-1970s, increasing attention has been directed toward the development and application of 3D stability models (Hovland 1977; Chen and Chameau 1983; Hungr 1987; Lam and Fredlund 1993; Huang et al. 2002). Many studies concerning identification of critical slip surface adopted a 3D model (Baker 1980; Celestino and Duncan 1981; Nguyen 1985; Li and White 1987; Bardet and Kapuskar 1989; Bolton et al. 2003).

So far, however, an easy implementation method of 3D analysis for practical issues is still lacking. Also, 3D deterministic model should be applied to a wide

mountainous area for the purpose of landslide hazard assessment with accurate prediction of the magnitude, the location, and the occurrence time of the dangerous process. Concerning the occurrence time of slope failure, the trigger factors of the occurrence of landslide, such as rainfall and earthquakes, should be taken into account.

For realizing these desires, some new technologies are essential. GIS, as a tool for geotechnical engineers, has capabilities that range from convenient data storage to complex spatial analysis and graphical presentation. Combing the conventional geotechnical methodologies with GIS will significantly enhance the slope stability analysis. As the earlier study of this topic, the authors (Qiu et al. 2006; Xie et al. 2006) proposed a GIS-based 3D slope stability analysis model which is derived from Hovland's model in order to calculate the 3D safety factor within GIS, and further used this model for locating the critical slip surface in a large area by means of minimizing the 3D safety factor.

This study evolved the proposed 3D model into an improved one by combining with an infiltration model, to evaluate the variation of slope stability during rainfall event, and developed an advanced GIS-based system to efficiently assess regional landslide hazard as well as identifying the location, the magnitude, and the occurrence time of slope failure.

5.2 Model Description

5.2.1 Mechanism of Rainfall-Induced Landslide

During heavy rains, water seeps into the ground and travels through unsaturated soils. This water may perch on lower permeability materials or a drainage barrier such as bedrock and highly impermeable clays, creating a temporary, localized saturated zone, calls wetting band. The wetting band approach (Lumb 1975) assumes that the wetting band descends vertically under the influence of gravity, until either the main water table or a zone of lower permeability (e.g., a clay stratum) is reached. When the descending wetting band reaches the main water table, the surface of the main water table will rise with an increase in pore pressure. Under the latter condition, a perched water table will form above the zone of lower permeability, and pore pressure will become positive. The perched water table is considered to be the key factor in triggering rainfall-induced slope failures, which are often shallow in nature.

The groundwater table is usually located at a considerable depth below the ground surface, and there is no evidence that heavy rainfall causes a rise in the water table sufficient to trigger shallow failures (Kim et al. 2004). Instead, this kind of failures may be attributed to the deepening of a wetting front into the slope due to rainfall infiltration which results in an increase in moisture content, a decrease in soil matric suction, and a decrease in shear strength on the potential failure surface

(Lumb 1975; Kim et al. 2004; Rahardjo et al. 1995; Ng and Shi 1998; Fourie et al. 1999). Therefore, when shallow failure of a soil slope is caused by rainfall, the mechanism is that water infiltration causes a reduction in soil suction (or negative pore pressure) in the unsaturated soil. Soil suction will be lost upon full saturation. This results in a decrease in the effective stress on the potential failure surface, which is reflected in a decrease in the soil strength to a point where equilibrium cannot be sustained in the slope. Also, during and after periods of prolonged intense rainfall, significant seepage forces may develop and add to the gravity-induced shear stress. Failure occurs under constant total stress and increasing pore pressure.

5.2.2 Infiltration Model

There are numerous models formulated on the basis of soil characteristics that have been proposed to evaluate infiltration (Green and Ampt 1911; Neuman 1976; Smith et al. 1993; Ogden and Saghafian 1997; Iverson 2000). However, it is still difficult to quantify the amount of infiltration and the corresponding effect on the stability of slope for a regional area due to the complex mechanism and many parameters that are used in the models. Those availabilities often require detailed geotechnical information on the existing conditions and long-time computation. Because of the high cost involved, they are generally only achievable at the site investigation level in cases where high risk is anticipated.

The Green and Ampt method (Green and Ampt 1911) remains popular to this day because of its succinct concept of the "piston" wetting front and the inclusion of soil suction head and hydraulic conductivity parameters. Four assumptions are made in this model: (1) Soil surface is maintained constantly wet by water ponding; (2) a sharp wetted front exists; (3) the hydraulic conductivity is constant through the soil; and (4) the soil matrix suction at the front remains constant. These assumptions mean that the soil is fully saturated from the surface to the depth of the wetting front, while the soil below the wetting front is at the initial degree of saturation.

According to Darcy's law, the infiltration rate is given by

$$f = K_s \frac{\psi_f + Z_f}{Z_f} \tag{5.1}$$

The depth of the wetting front can be related to the cumulative amount of infiltrated water by

$$F = Z_f(\theta_s - \theta_i) \tag{5.2}$$

Rearranging Eq. (5.2) to solve for Z_f and applying it to Eq. (5.1), the infiltration rate at any time t becomes

$$f(t) = K_s + K_s \frac{\psi_f(\theta_s - \theta_i)}{F} \tag{5.3}$$

The expression of $f(t)$ can be stated as follows:

$$t = t_p + \frac{1}{K_s}\left[F - F_p + \psi_f(\theta_s - \theta_i)\ln(n)\right] \tag{5.4}$$

$$n = \frac{\psi_f(\theta_s - \theta_i) + F_p}{\psi_f(\theta_s - \theta_i) + F} \tag{5.5}$$

t_p and F_p can be calculated from the following equations:

$$t_p = \frac{F_p}{P} \tag{5.6}$$

$$F_p = \frac{\psi_f K_s(\theta_s - \theta_i)}{P - K_s} \tag{5.7}$$

where $f(t)$ is the infiltration rate (m/h) at time t (h); K_s is the soil saturated hydraulic conductivity (m/h); ψ_f is the matrix suction at the wetting front (m); Z_f is the depth of the wetting front (m); F is the cumulative amount of infiltrated water (m); θ_s is the soil saturated volumetric water content; θ_i is the initial soil volumetric water content; t_p is the time when water begins to pond on the soil surface (h); F_p is the amount of water that infiltrates before water begins to pond at the surface (m); and P is the rainfall rate (m/h).

5.2.3 Applicability of GIS

A geographical information system, or simply GIS, has functional capabilities for data capture, input, manipulation, transformation, visualization, combination, query, analysis, modeling, and output (Bonham-Carter 1994). GIS is equipped with many functions that made GIS a powerful tool to model possible situations under various conditions given by specified data values or attribute values.

Recently, GIS has attracted great attention in landslide hazard assessment. The role of GIS in landslide analysis can be summed up as three aspects: data and/or analysis results expression, data handling, and data analyses (or modeling). However, from a survey of the recent applications of GIS to landslide hazard assessment, it is found that most researchers are concentrated in using a statistical method to quantify the relationship between slope failure and influential factors while GIS performs regional data preparation and processing; only a few researches, using infinite slope model which allows for calculation of a safety factor for each pixel individually to evaluate the stability of a specific-site slope, have been

conducted into the integration of GIS and the deterministic model (Anbalagan 1992; Dai et al. 2002; van Westen 1993). Although many engineers are familiar with GIS technology, they remain unaware of its analytical power and potential for wide and varied use. Since GIS enables more complex analysis of multiple data, it is expected that incorporating a sophisticated engineering model into GIS.

Most 3D limit equilibrium methods for slope stability analysis use column-based method in which the failure mass is divided into a number of small soil columns. Therefore, as shown in Fig. 5.1, it is possible to use grid-based columns, which are derived from overlaying GIS raster layers, to represent soil columns, that derived from discretization of the sliding mass (Qiu et al. 2006).

Based on the Mohr–Coulomb criterion, the safety factor of a slope failure mass is evaluated by comparison of the magnitude of the available shear strength with the shear strength required just to maintain stability along a potential failure surface. In a column-based 3D model, the available and required shear strength can be approximately calculated by summating corresponding items of all soil columns:

$$\mathrm{SF}_{3D} = \frac{\sum\limits_{J}\sum\limits_{I} F_{\mathrm{resistance}}(i,j)}{\sum\limits_{J}\sum\limits_{I} F_{\mathrm{sliding}}(i,j)} \tag{5.8}$$

where F_{3D} is the 3D safety factor; $F_{\mathrm{resistance}}(i, j)$, $F_{\mathrm{sliding}}(i, j)$ are the available and required shear strength function of the soil column (i, j) within the sliding mass, respectively; and I, J are number of rows and columns of the raster data within the sliding mass, respectively.
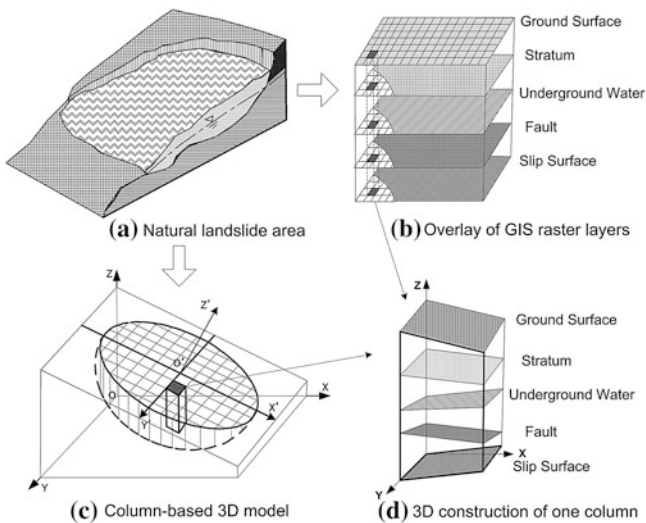

Fig. 5.1 Mechanism of GIS raster-based 3D model

The relevant items for calculation of safety factor should include elevation data of ground surface, slip surface, boundary of strata, and groundwater level (if it exists), and topographical parameters such as gradient and aspect of ground surface. In GIS, information of each item could be stored in a raster layer. Because a single raster layer can only represent certain information, it is not effective to treat so many raster layers at the same time. In contrast, vector data that comprise three geometry data types—point, line, and polygon—can describe many additional characteristics archived in an attribute table. Therefore, a point dataset is adopted here to manage the information of all raster layers. As shown in Fig. 5.2, the location of each point is set at the center of corresponding pixel of rater data, and the fields of the attribute table relate to each raster layer, respectively. The utilization of point dataset greatly expedites and simplifies the computation process for the safety factor.

5.2.4 Combination of Infiltration Model with 3D Slope Stability Model

Integrating Hovland's 3D model and the GIS raster data format, a new GIS-based 3D model has been proposed (Xie et al. 2006).

$$\mathrm{SF_{3D}} = \frac{\sum_J \sum_I \left[c'A + (W\,\cos\theta - U)\tan\phi\prime \right] \cos\theta_{\mathrm{Avr}}}{\sum_J \sum_I W\,\sin\theta_{\mathrm{Avr}} \cos\theta_{\mathrm{Avr}}} \tag{5.9}$$

where F_{3D} is the 3D safety factor of the slope; c' is the cohesion (kN/m^2); A is the area of the slip surface (m^2); W is the weight of one soil column (kN); $\phi\prime$ is the friction angle (°); θ is the inclination of the slip surface (°); θ_{Avr} is the angle between
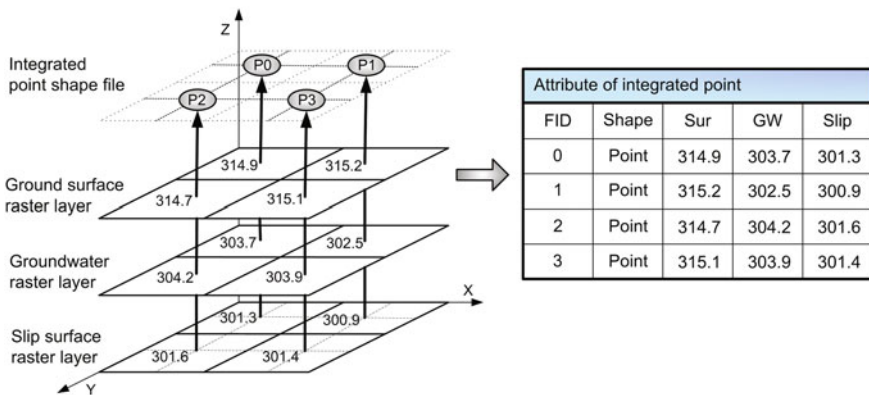

Fig. 5.2 Point dataset for integrating multiple raster layers

the direction of movement and the horizontal plane (°); and I, J are the numbers of rows and columns of the cell within the range of failure mass.

It is widely known that rainfall causes a rise of groundwater level as well as an increase in pore water pressure that results in slope failure. As mentioned above, the wetting front causes a reduction in soil suction (or negative pore pressure) and an increase in the weight of soil per unit volume. These result in a process in which soil resistant strength decreases while total stress increases, until failure occurs on the potential failure surface where equilibrium cannot be sustained.

Under these conditions, there are four possible situations regarding the slip surface that can be anticipated, and four models, based on the Eq. (5.9), are thus proposed to calculate the corresponding safety factors (Qiu et al. 2007).

Model 1: The slip surface forms in the unsaturated zone between the wetting front that is advancing from the ground surface and the groundwater table. In this situation, the horizontal resistance force and the horizontal sliding force acting on the slip surface can be calculated using Eqs. (5.10) and (5.11), respectively.

$$F_1 = \{c_i'A' + [\gamma_i z + (\gamma_{sat} - \gamma_i)H_w]A \cos\theta \tan\phi\prime\} \cos\theta_{Avr} \qquad (5.10)$$

$$F_2 = [\gamma_i z + (\gamma_{sat} - \gamma_i)H_w]A \sin\theta_{Avr} \cos\theta_{Avr} \qquad (5.11)$$

Model 2: The slip surface forms in the saturated zone between the ground surface and the wetting front that is advancing from the ground surface. In this situation, the horizontal resistance force and the horizontal sliding force can be calculated using Eqs. (5.12) and (5.13), respectively.

$$F_1 = [c_w'A' + (\gamma_{sat}z \cos\theta - u_w)A \tan\phi\prime] \cos\theta_{Avr} \qquad (5.12)$$

$$F_2 = \gamma_{sat}zA \sin\theta_{Avr} \cos\theta_{Avr} \qquad (5.13)$$

Model 3: The slip surface forms in the saturated zone under the groundwater table and the wetting front that has reached the groundwater table. The horizontal resistance force and the horizontal sliding force can be calculated using Eqs. (5.12) and (5.13), respectively.

Model 4: The slip surface forms in the saturated zone under the groundwater table and the unsaturated zone that exists between the wetting front and the groundwater table. In this situation, the horizontal resistance force and the horizontal sliding force can be calculated using Eqs. (5.14) and (5.15), respectively.

$$F_1 = \{c_w'A' + [(\gamma_i(z_w - H_w) + \gamma_{sat}(H_w + z - z_w)) \cos\theta - u_w]A \tan\phi\prime\} \cos\theta_{Avr}$$
$$(5.14)$$

$$F_2 = [\gamma_i(z_w - H_w) + \gamma_{sat}(H_w + z - z_w)]A \sin\theta_{Avr} \cos\theta_{Avr} \qquad (5.15)$$

Assuming that the vertical sides of each soil column are frictionless, the 3D safety factor can thus be calculated by summing F_1 and F_2 of all soil columns of failure mass.

$$\text{SF}_{3D} = \frac{\sum\limits_{J}\sum\limits_{I} F_1}{\sum\limits_{J}\sum\limits_{I} F_2} \tag{5.16}$$

where SF_{3D} is the 3D safety factor of the slope; F_1 is the horizontal resistance force (kN); F_2 is the horizontal sliding force (kN); γ_{sat} is the saturated unit weight of soil (kN/m^3); γ_i is the initial unit weight of soil (kN/m^3); c_i' is the initial effective cohesion of soil (kN/m^2); c_w' is the saturated effective cohesion of soil (kN/m^2); $\phi\prime$ is the effective friction of soil (°); Z_w is the depth of the wetting front (m); H_w is the depth of the groundwater table (m); Z is the depth of the slip surface (m); u_w is the pore stress (kN/m^2); A is the area of the soil column (m^2); A' is the area of the slip surface of the soil column; θ is the inclination of the slip surface (°); θ_{Avr} is the dip angle of the main sliding direction (°); and J, I are the numbers of rows and columns of the cell in the range of failure mass.

It should be noted that in Eq. (5.16), F_1 and F_2 of each soil column would be calculated using an appropriate equation that is selected from Eqs. (5.10) to (5.15) depending on the different conditions described above.

5.2.5 Search for Potential Slip Surface

Considering that many practical failure surfaces presented an ellipsoidal shape, in this study, the initial slip surface is assumed to be the lower portion of an ellipsoid.

Six parameters, namely three axial parameters "a, b, and c", the central point "C", the inclination angle "θ," and the inclination direction "Asp" of the ellipsoid, are selected to define the spatial posture of ellipsoid, as illustrated in Fig. 5.3.

Fig. 5.3 Definition of the spatial posture of ellipsoid
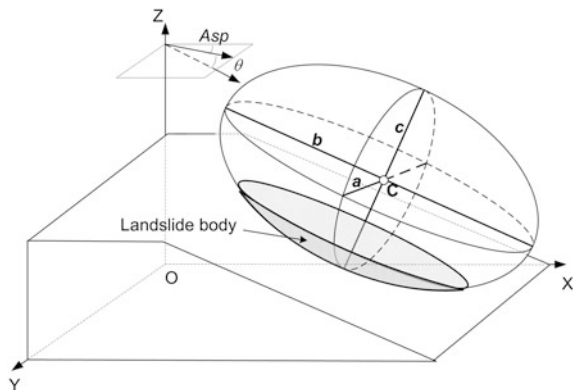
For implementing the critical slip surface searching, the random variables are firstly produced by Monte Carlo simulation to generate a random ellipsoid. The local posture of the ellipsoid is determined by the randomly selected central point and the coordinate conversion. The slip surface is identified by calculating the boundary surface of the lower part of the ellipsoid and the ground using the GIS raster data. Then, the 3D safety factor for each random trial slip surface can be calculated based on the GIS raster-based 3D model. After enough times of trial calculations, finally, the 3D critical slip surface and its associated safety factor can be obtained based on the minimum safety factor of trial calculations.

Each randomly produced slip surface is changed according to the different strata strengths and presence of weak discontinuities. If a randomly produced slip surface, based on the lower part of an ellipsoid, is lower than a weak discontinuous surface or the confines of the hard stratum, the weak discontinuity or the confined surface of the hard stratum will be prioritized for selection as one part of the assumed slip surface.

5.3   System Development

All of the analytic models have been modularized and incorporated into a standalone GIS system, called 3D slope stability analysis system (3DSSAS). Figure 5.4 is a simplified representation of the interaction between GIS and the 3DSSAS. All GIS functions that are used to perform the database construction, the analyses, and the result presentation are delivered from the Component Object Model-based GIS components assembly, ArcObjects. The main interface of 3DSSAS is shown in Fig. 5.5.

Figure 5.6 illustrates the basic architecture of 3DSSAS. The 3DSSAS system consists of six main modules:

(1) The 3D slope stability analysis module: This module contains three GIS raster-based 3D models, namely the 3D extension of Bishop's method, the 3D extension of Janbu's method, and the revised Hovland's method, and is used to calculate 3D safety factor of a specified sliding mass.

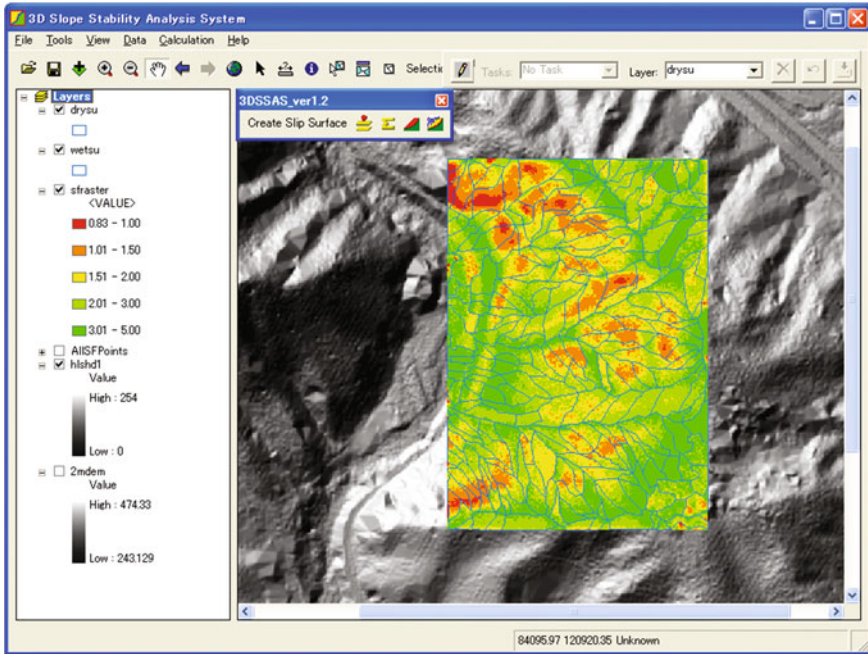**Fig. 5.4** Conceptual view of interactions between GIS and 3DSSAS
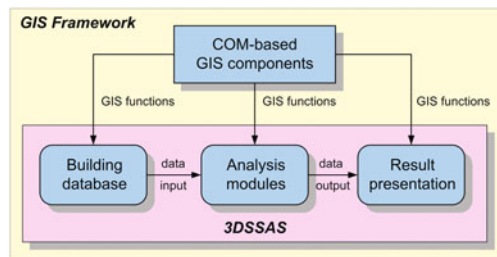
Fig. 5.5 Main interface of 3DSSAS

(2) The slip surface identification module: This module provides functions for simulating possible shape and posture of sliding mass and for locating critical slip surface by using the Monte Carlo simulating method.

(3) The slope-unit division module: By using this module, slope units are divided from DEM data, and subsequently, the topographical characteristics of slope units can be statistically calculated.

(4) The slope stability probabilistic analysis module: This module achieves the slope-unit-based probabilistic analysis aiming to slope stability estimate of a regional area, while maintaining the 3D deterministic model.

(5) The rainfall infiltration module: In this module, the temporal infiltration process of rainfall is quantitatively simulated by using an approximate formula of the Green and Ampt method.

(6) The rainfall-infiltration-integrated slope stability analysis module: The core module of the 3DSSAS system provides an integrated model that combined the infiltration model and the 3D slope stability analysis model to achieve the spatio-temporal estimation of shallow landslide hazard triggered by rainfall.

Besides these main modules, 3DSSAS also offers some useful functions, such as surface analysis functions, shapefile editing tool, and 3D viewer, for efficient data processing and result presentation. These modules are then combined together
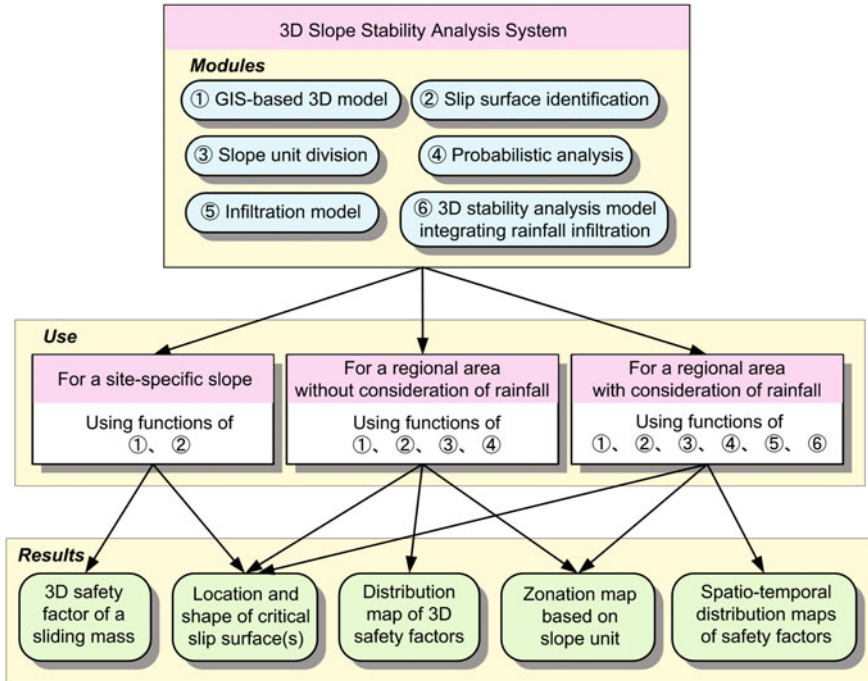
Fig. 5.6 Structure of 3DSSAS

effectively to enable the user to perform slope stability analyses in varying scales and under different conditions.

Analyzing the stability of a site-specific single slope with known slip surface is probably the simplest utilization of 3DSSAS. The prepared slip surface dataset is inputted into 3DSSAS with other necessary data. The 3D safety factor of this sliding mass is subsequently calculated by an appropriate 3D deterministic model that is provided by the slope stability analysis module. For the case of slip surface unknown, the slip surface identification module will be applied to perform randomly trial calculation to locate the critical slip surface by means of the minimum safety factor. The resultant data of slip surface is saved in raster format.

When targeting a regional area without rainfall effect considered, the slope-unit data is delivered firstly from the ground surface DEM data by using the slope-unit division module. For each slope unit, randomly trial calculations are performed by the slip surface identification module and the 3D slope stability analysis module to result in a series of slip surfaces with corresponding 3D safety factor. The critical slip surface is then extracted by means of the minimum safety factor and being saved into a polygon shapefile. The distribution of the 3D safety factors is saved as a raster data that are created by interpolation. Furthermore, the probabilistic analysis performed by the probabilistic analysis module for the distribution of the safety

factors delivers a reliability index, which is used to present the probabilistic stability of corresponding slope unit.

In the case of rainfall effect considered, in addition to the input data which are necessary for the analysis without rainfall considered, the rainfall data and the related hydraulic parameters are also needed for performance of the infiltration module. The spatio-temporal distribution of 3D safety factors is then derived by the rainfall-infiltration-integrated 3D slope stability analysis module.

The same as other engineering-aided software, the accuracy of the analytic result of 3DSSAS is data dependent. It raises a problem of the high cost involved in site investigation and indoor experiment for gathering detailed geotechnical information over a regional natural area. This is still a main difficulty in regional landslide hazard assessment.

In 3DSSAS, the evaluation of slope stability is based on the 3D safety factor. Basically, the calculation of the safety factor requires geometrical data (ground surface data, stratum data, and, if exists, and discontinuity data), data on the shear strength parameters (cohesion and angle of internal friction), and information on pore water pressure (groundwater data). Generally speaking, the best option for accomplishing an assessment is the application of 3DSSAS using all above-mentioned data with high precision, but is very cost demanding over large areas. Fortunately, using 3DSSAS, the ground surface data and the shear strength parameters which are the requisite minimum data are enough to complete a sketchy analysis. The ground surface data of a specific area can be conveniently obtained from aerial photographs or satellite images; the shear strength parameters could be obtained from test data or be estimated from geology. This paves a recommended way to a wise and efficient solution that using the requisitely minimal data, 3DSSAS allows a rapid assessment of stability in a given area to identify the parts where the possibility of occurrence of slope failure exists. The result of this kind of pre-analysis, even it is not exactly accurate, gives the information on possible location of landslide. The site investigation and indoor experiment can then be done purposefully for the possible locations, as well as subsequently detailed analysis.

5.4 Practical Application

National Route 49 runs from Iwaki city in Fukushima province to Niigata city in Niigata province, crossing Honshu Island, Japan. The Goto section, with a length of 1.3 km, is located about 10 km west of Iwaki city (Fig. 5.7), where slope disasters frequently occur and traffic regulations have to be issued during abnormal weather conditions. This seriously impacts on the use of the road. To evaluate the condition of slope stability and to support the decision-making process for suitable countermeasures, the 3DSSAS system was applied for landslide mapping.
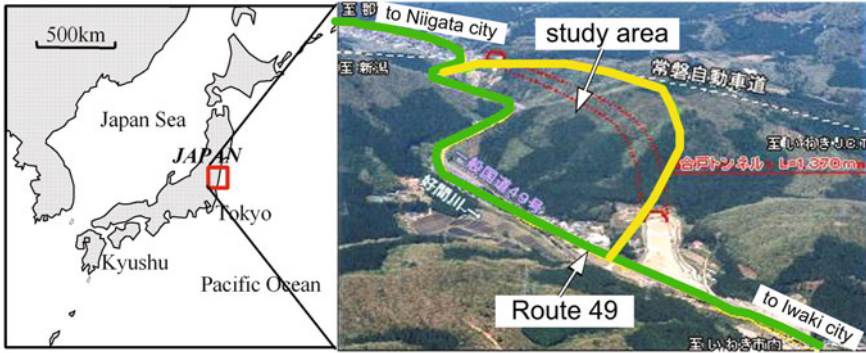
Fig. 5.7 Location of the Goto section of National Route 49

5.4.1 Description of the Study Area

The study area is located at the transition boundary between the eastern flat lands on the coast of the Pacific and the western Abukuma Plateau which is a late-Mesozoic metamorphic belt of the standard andalusite-sillimanite type. The area has a larger relative elevation of about 180 m compared to its surrounding area, and exhibits a morphology of U-shaped valley profile, with steep slopes in Mesozoic granites. The Route 49 runs beneath the slopes on the eastern side of the valley, along a north–south direction as shown in Fig. 5.7.

To obtain first-hand information about the engineering geological and geotechnical conditions regarding slope stability, a detailed field investigation was carried out for an area of 370 × 520 m on the upper slope of the Route 49, and this area is used as the study area of this research. The investigation results show that the granites are newly exposed in places over intermediate levels of the slope, which form very steep slopes with an angle greater than 50°, up to 70°. The upper slope is characterized by a relatively low-gradient terrain with a covering of quaternary deposits. Similar terrain is exhibited at lower levels of the slope, covered by colluvium and residual deposits formed by weathering of granites and accumulation of debris as result of landslide activities.

A field landslide mapping was performed for a part of the investigated area. Figure 5.8 shows this landslide map and summarizes the main geomorphological features of this area. A few old trails of soil creep, in a width of 10–15 m, are found at middle and near upper levels of the slope where the depth of the soil cover is greater than 2 m. Meanwhile, relatively fresh trails of landslides, in a smaller width of 5–10 m, are frequently seen at middle slope with underneath granites exposed, and at lower part of the slope where residual deposits underlaid.
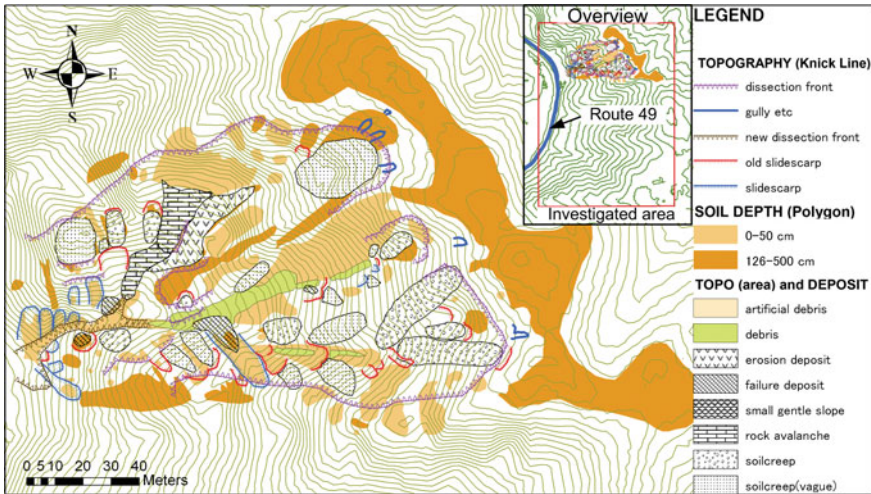
Fig. 5.8 Field investigation map showing the landslides occurring in the study area

5.4.2 Data Collection and Preparation

For a larger range of 1 × 1 km, a surface DEM dataset in grid form with 2 m mesh size was obtained by an airborne laser scanning. Figure 5.9 shows this DEM dataset with overlaying the range of the study area. The distribution of the slope angle is subsequently generated by corresponding GIS analytic function, in the same grid form as the DEM's. The result shows that in the range of the study area, the maximum slope angle is 69° with a mean of 31° and a standard deviation of 12.74, which is in agreement with the field observation. In addition, during the field investigation, a special surveying method was carried out to obtain the detailed data for soil depth in the study area. The bedrock surface was then constructed as a GIS raster dataset by subtraction of the soil depth from the surface elevation. Figure 5.10 shows a 3D view of the topography of the bedrock surface with the ground surface cover.

The physical properties and the mechanical behaviors of the soils in the study area have been studied by laboratory tests that include a permeability test and triaxial compression tests, for soil samples collected from three different spots. Due to the little variance in value of the test result of three soil samples, an average value of each geomechanical parameter of the surficial soil is used for the whole study area, as the c (cohesion), ϕ (friction angle), and γ (unit weight) are 2.0 kN/m^2, 41°, and 15.3 kN/m^3, respectively. Because there is no field groundwater level monitoring, the influence of the groundwater on slope stability was ignored in this study.

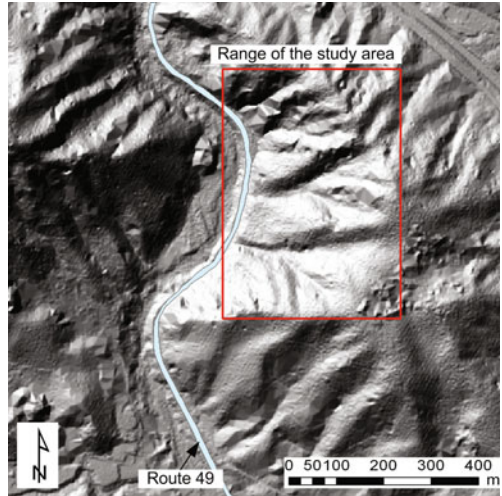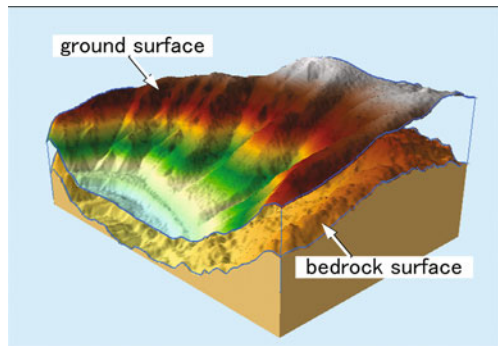**Fig. 5.9** DEM dataset with overlaying the range of the study area

Fig. 5.10 3D view of the bedrock surface with ground surface covering

5.4.3 Analysis and Evaluation

The Monte Carlo calculation was then used to map the distribution of 3D safety factors and to detect the critical slip surfaces. Because the soil cover in the area is composed mainly of colluvium and residual deposits formed by weathering of granites underneath, according to the characteristics of the geological formation, the possible collapse mode is considered to be a shallow slope failure with a sliding surface along the boundary surface of the bedrock or within the soil layer. Hence, in the trial search process, if the lower part of a randomly produced ellipsoid is lower than the boundary surface of the bedrock, the surface of the bedrock will be prioritized for selection as part of the assumed slip surface. Considering the time consumed and effectiveness, the number of calculations in the Monte Carlo simulation for one center point was set to 100, which taking around 8 s.

After the trial calculation, 100 values of the 3D safety factor were obtained for each center point. The distribution of the resultant safety factors of each point tends to be lognormal. In this study, the minimum value of the resultant safety factors, which reflects the maximum degree of danger, was used as the final result of the 3D safety factor of the center point.

Assuming that the resultant 3D safety factors of all center points have a PDF that corresponds to a lognormal distribution, a reliability index was then calculated for each slope unit. The zonation map of slope stability was thus obtained. Figure 5.11 shows this slope-unit-based zonation map, which can stochastically represent the sensitivity to slope failure of the study area. The lognormal distribution of 3D safety factors of two slope units, which are labeled as slope unit 129 and 20 in Fig. 5.11, is shown in Fig. 5.12. It is seen that slope unit 129 has a mean safety factor of 1.382, and slope unit 20 has a higher safety factor of 1.528. In a deterministic sense, it would appear that slope unit 20 is safer than slope unit 129. However, the safety factor PDF for slope unit 129 has a much smaller standard deviation in comparison with slope unit 20, which leads to a reliability index value of slope unit 129 of 2.454, while that of slope unit 20 is 1.377. So slope unit 129 is considered safer than slope unit 20 as there is less uncertainty associated with slope unit 129. On the basis of Table 5.1, slope unit 129 would be descriptively classified as "poor" and slope unit 20 would be assigned a "hazardous" rating.

For the study area, a uniform rainfall event with duration of 10 h and an intensity of 8 cm/h was assumed, and the method proposed above was applied. The detection of critical slip surfaces was achieved through trial searching and calculation of the 3D safety factor. In the trial searching process, if the lower part of a randomly

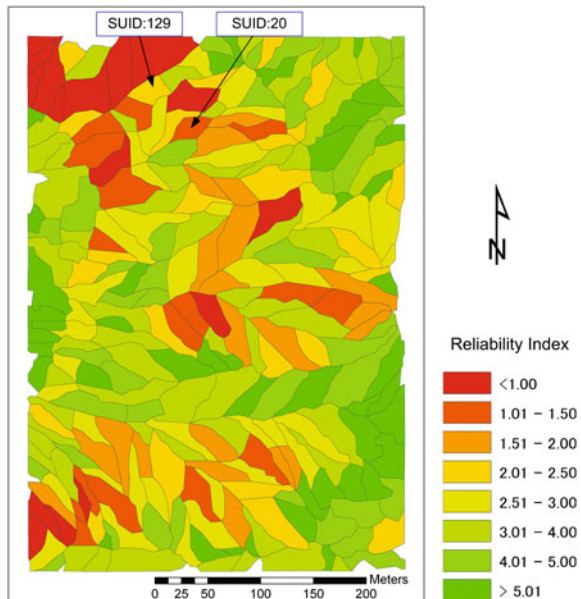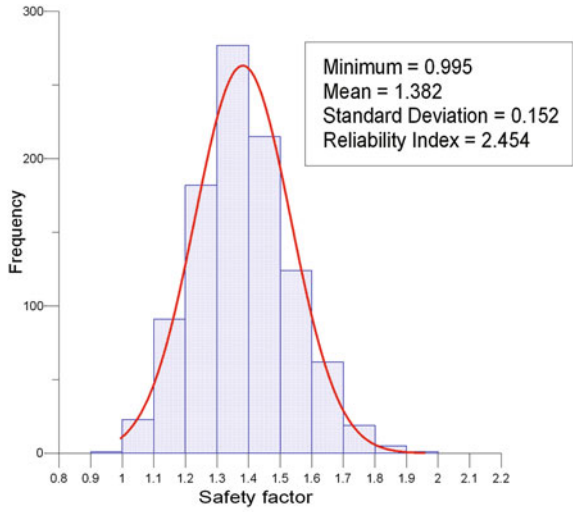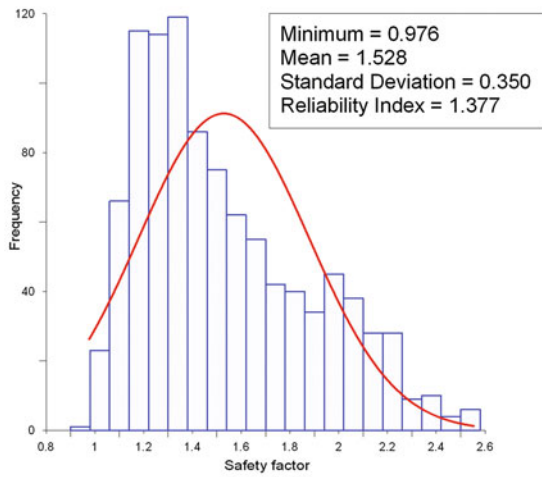**Fig. 5.11** Slope-unit-based landslide hazard zonation map

Fig. 5.12 Distribution of 3D safety factors of two slope units

(a) SUID:129

(b) SUID:20

Table 5.1 Example values of β and P_F

Performance level	Reliability index β	Probability $P_F = P(F < F_c)$
High	5.0	2.871×10^{-7}
Good	4.0	3.169×10^{-5}
Above average	3.0	0.00135
Below average	2.5	0.00621
Poor	2.0	0.02275
Unsatisfactory	1.5	0.06681
Hazardous	1.0	0.15866

produced ellipsoid is lower than the boundary surface of the bedrock, the confined surface of the bedrock will be prioritized for selection as one part of the assumed slip surface.

After 100 trial calculations for each raster cell taken as the central point of a trial ellipsoid in the study range, finally, the variation of safety factors over time was mapped. Figure 5.13 illustrates six distribution maps of the safety factors changing over time. From these maps, a high correlation between rainfall and the decrease of the safety factor can be recognized. The calculating result, however, presents slight overestimation for the possibility of failure occurrence as the lowest safety factor was nearly 0.4. The reason was considered as the presumption of the constantly high intensity of rainfall event which actually seldom, if not never, occurs in the reality. Also, the neglect of the lateral outflow of infiltrated water in the infiltration model is another reason that derived the overestimation of failure possibility.

5.5 Concluding Remarks

In this study, responding to the question regarding the occurrence time of slope failures, a challenge has been done for dealing with deterministic slope stability analysis related to shallow rainfall-induced landslides. A new 3D slope stability model was developed by coupling a dynamic hydrological model that simulates the rainfall infiltration over time with the developed 3D slope stability model that quantifies the varying safety factor during rainfall. Using this model, the location and the magnitude of potential failures can be identified through a random search procedure for minimizing 3D safety factor; furthermore, the time of occurrence of failures can be forecasted by mapping the changing distribution of safety factors during rainfall.

For typical slopes, the material is originally unsaturated and the surface of the slope is continuously being wetted by rainfall. Short heavy rainfall after a prolonged dry period cannot create the conditions leading to saturation, while a heavy rainfall after a period of moderate rainfalls may saturate the remaining upper few inches of unsaturated soil. Hence, the consideration concerning the antecedent rainfall would be necessary, although is uncompleted at the present stage in this study, for simulating a gradual buildup of moisture in the ground over a prolonged period of time. In addition, owing to limited data about rainfall records related to occurrence times of landslide, calibration and validation of the model are difficult.

Incorporating all proposed technologies and models, a comprehensive GIS-based system, called 3D slope stability analysis system (3DSSAS), has been developed for efficiently assessing and mapping regional landslide hazard. Once necessary data, including slope-related data and hydraulic data, are acquired, this system is shown to have the abilities both to estimate the variation of slope stability over a wide natural area during rainfall which answers the question about occurrence time of failures and to identify the location and shape of potential failure surfaces which answers the questions of location and magnitude. The effectiveness

Fig. 5.13 Distribution maps of safety factors changing over time
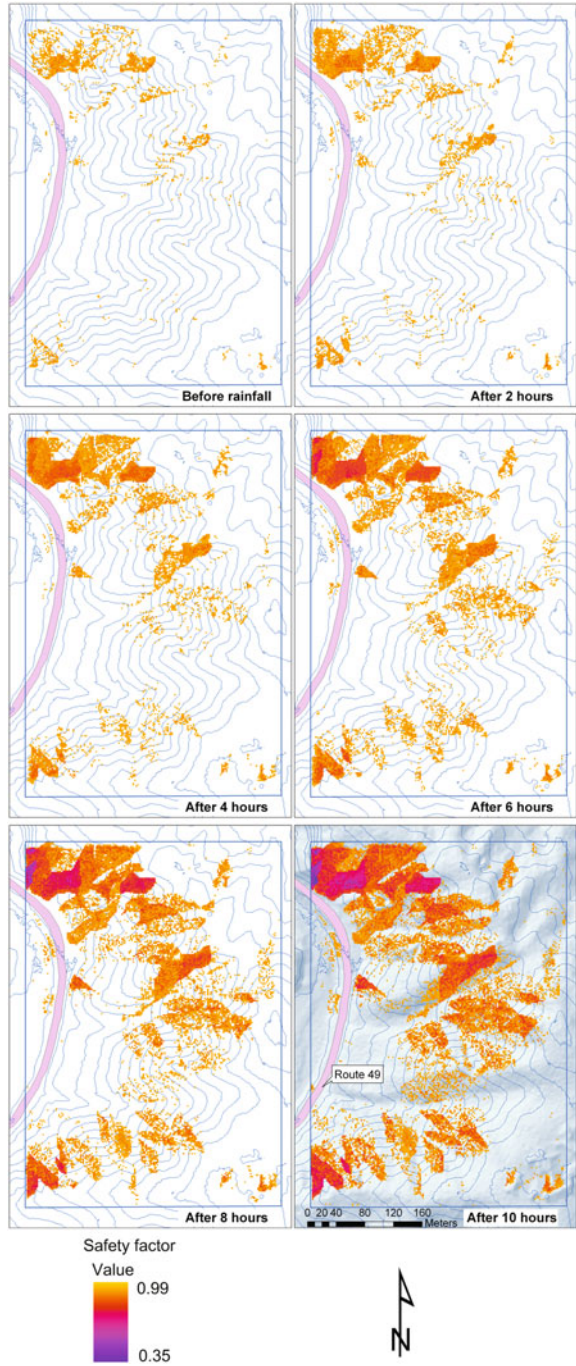
of the system has been tested by two practical applications for landslide-prone area in Japan.

3DSSAS was designed to be an architecture that has capabilities to implement multiple purposes by interconnecting appropriate models and technologies to be a subsystem. For instance, the stability of a specific slope with a known slip surface can be quantified by means of the 3D safety factor using the 3D slope stability analysis model; techniques of slope-unit division and slip surface location would be used with the 3D mode together for a regional assessment; and, when rainfall is considered as a trigger factor, the hydraulic model should be added.

Landslide hazard is considered a continuous, spatially aggregated variable. Natural slopes that have been stable for many years may suddenly fail because of changes in topography, seismicity, groundwater flows, and weathering. Hence, the renewal of the data would result in a different assessment for same site. With the fast development in geoinformation science and earth observation, there are more and more tools available for quickly data acquisition. For example, high resolution remote sensing products can be used to derive DEMs in any desired time period. Based on these considerations, besides being robust for a reliable landslide hazard assessment, the developed system also provides powerful capabilities for data processing and easy application to quickly reestablish the hazard assessment at any time responding to data renewal.

The accuracy of landslide assessment systems is generally data dependent. A comprehensive and exhaustive evaluation of landslide hazard often requires detailed and accurate datasets about the spatial variation of parametric values which form the input of the slope stability and hydrological models. However, the spatial distribution of these datasets is extremely difficult to measure. Material properties are also difficult to measure for many points over large areas and show a high spatial variability. At the present stage, because of the high cost involved, they are generally only achievable at the site investigation level in cases where high risk is anticipated. Responding to this problem, a cost–benefit solution given by this study is that a sketchy evaluation for whole studying area, even maybe being a little inaccuracy, can be firstly completed by 3DSSAS using the most sensitive parameters consists of DEM (which can easily be obtained from accurate aerial photographs or satellite survey data nowadays) and geomechanical parameters (which can be empirically supposed from various sources such as a existing geology map), in order to select areas with relative high susceptibility related to failure occurrence for more detailed investigation. Based on the detailed investigation available for specific slopes, stricter analysis can then be performed with detailed data to quantify the possibility with higher precision. It is believed that the analysis would end in more accurate results when the number and precision of parameters increase.

On the other hand, considering that the limitations in the theory and the parameterization of the analytic models leave many uncertainties concerning the absolute value of the 3D safety factor, a slope-unit-based probabilistic method was proposed by combining the Monte Carlo calculations with probabilistic statistics related to the variability of the 3D safety factors distributed in each slope unit to result in a reliability index as the probability of failure. The final result of such an

approach is a zonation of the entire area into landslide hazard units. The same probability of experiencing landslides is given to the entire slope unit; however, abrupt changes may occur between adjacent units.

Due to the insufficiencies in data acquisition and handling, and uncertainties in model selection and calibration, the validation of the developed system is still lack. In general, predictive models of landslide hazard can not be readily tested by traditional scientific methods. Indeed, the only way a landslide predictive map can be validated is through time.

With the fast development in earth observation science and geotechnics, there are more and more techniques available for carrying out a more reliable and quickly landslide hazard assessment. For example, high resolution remote sensing products can be used to derive DEMs in any desired time period for reassessing the landslide hazard at any time. Using these technologies, a comprehensive and advanced system can be established. In such a system, real-time monitoring data on rainfall, earthquake, pore pressure, and displacement of landslides, which may be a trigger for landslide occurrence, or indications of the movement of specific landslides, should be communicated into the database in real time for the purpose of landslide warning. This information can be acquired at sites by local monitoring units and be transmitted to management center by network links. Once the spatial database has been developed, the manipulation and analysis of the data allow it to be combined in various ways to evaluate what will happen in certain situations. The overlay operation of the GIS allows experts to combine the analytic results with factor maps of site characteristics in a variety of ways to produce landslide hazard maps to distribute.

Although due to the limitations of time and techniques, some concepts of this study are still unaccomplished; it is hoped that this study may be helpful to provide a rational framework for future research work and will present some aid to other researchers in the field of landslide hazard assessment.

References

Anbalagan R (1992) Terrain evaluation and landslide hazard zonation for environmental regeneration and land use planning in mountainous terrain. Proc. VI Int Symp On landslides, vol 2. Christchurch, New Zealand, pp 861–868

Baker R (1980) Determination of the critical slip surface in slope stability computations. Int J Numer Anal Methods Geomech 4:333–359

Bardet JP, Kapuskar MM (1989) A simplex analysis of slope stability. Comput Geotech 8:329–348

Bonham-Carter GF (1994) Geographic information systems for geoscientists: modeling with GIS. Pergamon, Ottawa, 398 pp

Bolton Hermanus PJ, Heymann G, Groenwold A (2003) Global search for critical failure surface in slope stability analysis. Eng Opt 35(1):51–65

Celestino TB, Duncan JM (1981) Simplified search for non-circular slip surface. Proceedings of the 10th international conference on soil mechanics and foundation engineering, Stockholm, Sweden, pp 391–394

Chen RH, Chameau JL (1983) Three-dimensional limit equilibrium analysis of slopes. Geotechnique 32(1):31–40

Chang M (2002) A 3D slope stability analysis method assuming parallel lines of intersection and differential straining of block contacts. Can Geotech J 39:799–811

Dai FC, Lee CF, Ngai YY (2002) Landslide risk assessment and management: an overview. Eng Geol 64:65–87

Fourie AB, Rowe D, Blight GE (1999) The effect of infiltration on the stability of the slopes of a dry ash dump. Geotechnique 49(1):1–13

Green WH, Ampt GA (1911) Studies of soil physics: I. The flow of air and water through soils. J Agric Sci 4:1–24

Hovland HJ (1977) Three-dimensional slope stability analysis method. J Geotech Eng Div, ASCE 103(GT9):971–986

Hungr O (1987) An extension of Bishop's simplified method of slope stability analysis to three dimensions. Geotechnique 37(1):113–117

Huang C, Tsai C, Chen Y (2002) Generalized method for three-dimensional slope stability analysis. J Geotech Geoenviron Eng 128(10):836–848

Iverson RM (2000) Landslide triggering by rain infiltration. Water Resour Res 36(7):1897–1910

Kim J, Jeong S, Park S, Sharma J (2004) Influence of rainfall-induced wetting on the stability of slopes in weathered soils. Eng Geol 75:251–262

Lumb P (1975) Slope failures in Hong Kong. Q J Eng Geol 8:31–65

Li KS, White W (1987) Rapid evaluation of the critical slip surface in slope stability problems. Int J Numer Anal Methods Geomech 11:449–473

Lam L, Fredlund DG (1993) A general limit equilibrium model for three-dimensional slope stability analysis. Can Geotech J 30:905–919

Neuman SP (1976) Wetting front pressure head in the infiltration model of Green and Ampt. Water Resour Res 12(3):564–566

Nguyen VU (1985) Determination of critical slope failure surface. J Geotech Eng, ASCE 111 (2):238–250

Ng CWW, Shi Q (1998) A numerical investigation of the stability of unsaturated soil slopes subjected to transient seepage. Comput Geotech 22(1):1–28

Ogden F, Saghafian B (1997) Green and Ampt infiltration with redistribution. J Irrig Drainage Eng 123(5):386–393

Qiu C, Esaki T, Xie M, Mitani Y, Wang C (2006) New implementation approach of three-dimensional slope stability analysis using geographical information system. In: Leung CF, Zhou YX (eds) Rock mechanics in underground construction, the 4th Asian rock mechanics symposium. World Scientific Publishing, Singapore, 488 pp

Qiu C, Esaki T, Xie M, Mitani Y, Wang C (2007) Spatio-temporal estimation of shallow landslide hazard triggered by rainfall using a three-dimensional model. Environ Geol 52:1569–1579

Rahardjo H, Lim TT, Chang MF, Fredlund DG (1995) Shear strength characteristics of a residual soil. Can Geotech J 32:60–77

Smith RE, Corradini C, Melone F (1993) Modeling infiltration for multistorm runoff events. Water Resour Res 29:133–144

Varnes DJ (1984) Landslide hazard zonation: a review of principles and practice. IAEG Commission on Landslide and other Mass-Movements. UNESCO press, Paris, 63 pp

van Westen CJ (1993) Application of geographical information system to landslide hazard zonation. ITC Publication no. 15, ITC, Enschede, The Netherlands, 245 pp

Xie M, Esaki T, Qiu C, Wang C (2006) Geographical information system-based computational implementation and application of spatial three-dimensional slope stability analysis. Comput Geotech 33:260–274